Biointerface Research in Applied Chemistry
Open-Access Journal (ISSN: 2069-5837)

Article
Volume 16, Issue 3, 2026, 98
https://doi.org/10.33263/BRIAC163.098

Investigation of the *In Silico* and Biological Activities of Substituted Phenethylamine-Based Imine-Metal Complexes

Taha Yasin Bayram [1], Merve Yildirim [2], Elif Aksakal [2], Bunyamin Ozgeris [3,*], Arzu Gormez [4]

1 Department of Molecular Biology and Genetics, Faculty of Science, Ataturk University, 25000, Erzurum, Türkiye; tahayasin.bayram20@ogr.atauni.edu.tr (T.Y.B.);
2 Department of Molecular Biology and Genetics, Faculty of Science, Erzurum Technical University, 25000, Erzurum, Türkiye; merve.yildirim15@erzurum.edu.tr (M.Y.); elif.aksakal47@erzurum.edu.tr (E.A.);
3 Department of Basic Sciences, Faculty of Science, Erzurum Technical University, 25000, Erzurum, Türkiye; bunyamin.ozgeris@erzurum.edu.tr (B.O.);
4 Department of Biology, Faculty of Science, Dokuz Eylul University, 25000, İzmir, Türkiye; arzu.gormez@deu.edu.tr (A.G.);
* Correspondence: bunyamin.ozgeris@erzurum.edu.tr;

Received: 5.02.2026; Accepted: 20.05.2026; Published: 15.06.2026

Abstract: Imines are biologically active compounds formed by primary amine-carbonyl condensation, coordinating through the C=N group. Here, copper(II) and zinc(II) complexes of a novel imine ligand were synthesized and evaluated for their multi-targeted biological potentials. Although lacking antimicrobial activity, both complexes demonstrated dose-dependent antioxidant activity in DPPH, ABTS, and CUPRAC assays (IC_{50} ranges: 0.47508-0.63325 mg/mL). Supported by in silico docking studies showing targeted binding affinities ranging from -10.2 to -6.7 kcal/mol against critical protein targets. Anticancer and cytotoxic effects were assessed in A549 and HDF-1 cells using the WST-8 and SRB assays. Both imin-metal complexes exhibited moderate anticancer activity in A549 cells, with the Cu complex having an IC_{50} value of 42.27 ± 0.68 µM and the Zn complex having an IC_{50} value of 45.21 ± 0.34 µM. While the Cu complex showed a cytotoxic effect at high concentrations in HDF-1 cells (IC_{50}: 167.13 ± 0.15 µM), the Zn complex exhibited a high cytotoxic effect (IC_{50}: 5.09 ± 0.03 µM) at all tested concentrations (6.25-200 µM). As a result of the SRB analysis, the total protein amount in A549 cells was determined to be 56% and 63% for Cu and Zn complexes, respectively; in HDF-1 cells, it was determined to be 94% and 11%, respectively.

Keywords: imines; metal complex; antimicrobial activity; anticancer activity; antioxidant activity.

1. Introduction

Imines (Schiff bases) are organic compounds containing a central azomethine (C=N) group, formed by the acid-catalyzed reversible condensation of primary amines with aldehydes or ketones [1]. Due to their ease of synthesis, high yields, electronic flexibility, and coordination capabilities, these structures serve as powerful ligands. They are widely used in medicine, biomaterials, catalysis, industry, and materials science. The reversible and pH-sensitive nature of imine bonds allows for the development of self-healing smart networks and

functional hydrogels through their hydrolysis properties; while additional conjugations, such as aromatic rings or –C═C– bonds, influence reactivity and surface adsorption, intramolecular hydrogen bonds impart high stability to the crystal structure [2]. In coordination chemistry, imines bind metals through donor atoms, such as imine nitrogen and phenolic oxygen, thereby finely tuning the electronic structure and geometry (e.g., octahedral, tetrahedral, or square pyramidal) of the complexes depending on the metal center and substituents [3]. By enhancing DNA binding and redox properties through metal coordination, these complexes exhibit various biological activities, including anticancer, antibacterial, antifungal, and antioxidant effects, making them valuable for medical and biomedical applications such as pharmacophore small molecules, controlled drug delivery, wound-healing systems, and biocompatible coatings [4,5].

Imines and their transition-metal complexes represent a crucial class of compounds in biochemistry and pharmaceutical chemistry due to their significant antioxidant potential, which plays a vital role in protecting biological systems from oxidative stress damage caused by the overproduction of free radicals [6]. These free radicals can cause irreversible damage to lipids, DNA, and proteins, contributing to the etiology of various diseases; therefore, synthetic antioxidants such as Schiff base complexes offer a promising therapeutic and preventive alternative [7]. The importance of these complexes is further underscored by the synergistic effect between the metal ion and the ligand, in which coordination often enhances radical scavenging activity by redistributing the electronic cloud and activating the ligand's π system [8]. Consequently, because they can stabilize various oxidation states and enhance bioactivity, Schiff base metal complexes are promising candidates for the development of new antioxidant agents that bolster the body's resistance to disease [9].

Imine and metal complexes hold a critical position in pharmaceutical science and drug discovery due to their broad spectrum of antimicrobial activities, including antibacterial, antifungal, and antiviral properties. The core importance of these compounds lies in the presence of the azomethine (-C=N-) group, a privileged pharmacophore that interacts with cellular active sites through hydrogen bonding to inhibit microbial growth [10]. Furthermore, their ability to form stable metal complexes through chelation significantly enhances their biological potency by increasing lipophilicity and improving cell membrane penetration compared to the parent ligands. Given the global rise in antibiotic resistance, Schiff bases represent a promising scaffold for developing novel, effective therapeutic agents to treat various infectious diseases [11].

Schiff base metal complexes have emerged as a critical domain in medicinal chemistry due to their remarkable potential as versatile anticancer agents. Recognized as “privileged ligands,” Schiff bases effectively stabilize transition metals in various oxidation states, enhancing the complexes’ lipophilicity and facilitating their penetration into the lipid bilayer of target cell membranes [12,13]. The therapeutic significance of these compounds is underscored by their multifaceted mechanisms of action, which include selective binding to nuclear or mitochondrial DNA, the generation of intracellular reactive oxygen species (ROS), enzyme inhibition, and the induction of apoptotic pathways Furthermore, many of these complexes demonstrate superior selectivity and the capacity to overcome multidrug resistance, offering a promising alternative to conventional platinum-based drugs that are often limited by systemic toxicity and clinical resistance [13]. Consequently, the structural modifiability and potent biological activity of Schiff base metal complexes position them as essential candidates for the development of advanced anticancer metallodrugs [14].

Considering the biological importance of imine-metal complexes, the aim was to synthesize, characterize, and evaluate the biological activities of new substituted phenethylamine-based imine-metal complexes. Although the literature reports that imine-metal complexes can exhibit antioxidant, antimicrobial, and anticancer properties, studies specifically examining the diverse biological effects of phenethylamine-based imine-metal complexes are limited. In this context, the antimicrobial, antioxidant, and anticancer/cytotoxic potentials of the synthesized Cu(II) and Zn(II) complexes were investigated using different biological test systems. In this regard, it is thot that the study will provide new contributions to the literature on the biological activities of phenethylamine-based imine-metal complexes.

2. Materials and Methods

2.1. Materials.

The chemical reagents required for synthesis, including Benzaldehyde, Methylene Chloride, Molecular Sieve 4(Å), Triethylamine, Chloroform D1, Ethanol, Copper (II) Chloride Dihydrate, and Zinc Chloride, were procured from Sigma Aldrich. 4-Methyl Phenethylamine and 4-Methoxy Phenethylamine were sourced from Acros Organics and J&K Scientific, respectively, while n-Hexane was supplied by TEKKİM. To conduct antioxidant activity evaluations, ascorbic acid, neocuproine (Isolab), ammonium acetate (Sigma-Aldrich), ABTS (Fluka), and potassium persulfate (K2S2O8) (Carlo Erba) were obtained. Microorganism growth and antimicrobial testing were performed using Mueller-Hinton Agar (MHA) (Oxoid), Mueller-Hinton Broth (MHB) (Biolife), Luria-Bertani Agar (LBA) (Miller MERCK), Potato Dextrose Agar (PDA) (Oxoid), and DMSO (Merck). Moreover, components for anticancer experiments, namely DMEM (Biowest), RPMI-1640 (Ecotech), FBS (Gibco), L-Glutamine (WISENT INC), PenStrep (Gibco), PBS (Gibco), Trypsin/EDTA (Gibco), and CVDK-8 (Ecotech), were successfully acquired. The characterization of the chemical structures was accomplished using XRD and IR spectroscopy. A range of 4000-400 cm^{-1} was scanned to acquire IR spectra on an IRTracer-100 FTIR spectrophotometer. Powder X-ray diffraction data were gathered using an EMPYREAN diffractometer system, which features a Cu X-ray source λ=1.5406 Å). Electronic absorption (UV-Vis) spectra were recorded at room temperature on a Shimadzu UV-3600 Plus UV-Vis-NIR spectrophotometer using quartz cuvettes with a 1.0 cm path length.

2.2. Methods.

2.2.1. Synthesis dizayn.

2.2.1.1. Imin synthesis based on (E)-N-benzylidene-2-(4-methoxyphenethyl)ethanamine (3).

To prepare the target imine (3), benzaldehyde (1) (0.500 g, 1 eq.) and 4-Methoxyphenethylamine (2) (1.06 g, 1 eq.) were combined in a 100 mL beaker in the presence of 1.0 g of molecular sieve (4Å). The resulting mixture was agitated using a glass rod until an exothermic reaction (warming) was observed. Subsequently, 20 mL of methylene chloride was added to the beaker, and the mixture was filtered through filter paper. The solvent, methylene chloride, was then eliminated via a rotary evaporator. The crude product underwent crystallization from a hexane-methylene chloride solvent mixture, affording imine (3) as distinct yellow crystals with an 89.52% yield (1.01 g) [15].

2.2.1.2. General synthetic procedure for imine–metal complexes (4–5)

To prepare the metal solutions, individual metal salts, Copper (II) Chloride Dihydrate and Zinc Chloride (1 eq.), were dissolved in 15 mL of ethanol and dried over 1.0 g of molecular sieve (4Å) at ambient temperature for 30-40 min. Parallelly, the imine ligand (2 eq.) was introduced into a 250 mL two-neck round-bottom flask containing 15 mL of ethanol. An inert atmosphere was established within the reaction vessel using nitrogen (N2) gas. After the inert conditions stabilized, the pre-dried metal salt solutions were transferred dropwise into the flask, followed by the addition of triethylamine (2 eq., 0.72 mL). The resulting mixture was refluxed at 100°C overnight. Upon completion of the reflux period, the reaction mixture was transferred to sterile centrifuge tubes and centrifuged at 9000 rpm for 15 min. After discarding the supernatant, the remaining solid precipitate was washed with ethanol (10 mL) and centrifuged once more under identical conditions (9000 rpm, 15 min). The isolated solid particles were allowed to dry at room temperature. This procedure afforded the imine-copper complex (4) as a brown solid in 69% yield (0.389 g) and the imine-zinc complex (5) likewise as a brown solid in 88% yield (0.497 g) [16].

2.2.2. Antibacterial Screening via Disc Diffusion

To determine the antibacterial sensitivity of the metal complexes (4-5), a standard disc diffusion test was performed. Bacterial suspensions, calibrated to the 0.5 McFarland standard, were spread onto petri dishes. Paper discs were impregnated with 10 µL of the complex solutions (200 µM) and carefully placed onto the seeded agar. The petri dishes were then incubated at 37°C, and the diameters of the inhibition zones were measured after 24 hours. The entire screening process was conducted in triplicate for validation, with 1% DMSO as the negative control. All tests were performed in triplicate. 1% DMSO was used as a negative control [17].

2.2.3. Antioxidant activity studies.

2.2.3.1. ABTS radical scavenging activity.

The spectrophotometric assessment of antioxidant activity is based on the reduction and subsequent decolorization of the blue-green ABTS.+ radical cation in the presence of scavenging agents. Initially, the radical solution was prepared by mixing 7 mM ABTS and 2.45 mM potassium persulfate (1:1 ratio), followed by a 12–16 hour incubation in the dark at room temperature. Ethanol was then used to dilute the mixture to achieve a target absorbance of 0.7 ± 0.02 at 734 nm. Aliquots of the metal complex solutions (10 µL) at concentrations ranging from 6.25 to 200 µM were added to 1 mL of the diluted ABTS reagent. After allowing the reaction to proceed for 6 minutes at room temperature, spectrophotometric absorbance was monitored at 734 nm. While DMSO served as a negative control, Trolox and ascorbic acid were included as standard benchmarks. All tests were performed in triplicate, and the results were averaged [18].

2.2.3.2.Cupric reducing antioxidant capacity (CUPRAC).

The established Cu2+ reduction test was used to assess the electron-donating capacity of the synthesized complexes. To individual samples of the complexes prepared at different concentrations (6.25-200 µM), a mixture composed of 0.25 mL of 0.01 M CuCl2, 0.25 mL of

methanolic neocuproine (7.5×10^{-3} M), and 0.25 mL of 1 M ammonium acetate buffer was added. All tests were performed in triplicate. Ascorbic acid and Trolox were used as a standard. DMSO was used as a negative control. The reaction mixture was brought to 2 mL with dH2O. After a 30-minute mixing period, the final absorbance was recorded at 450 nm using a spectrophotometer [19].

2.2.3.3. DPPH radical scavenging activity.

This method was used to evaluate the free-radical-quenching potential of the synthesized compounds. A 1 mM DPPH solution was prepared in methanol. To 50 µL of metal complex solutions prepared at different concentrations (6.25-200 µM), 100 µL of methanol, and 50 µL of DPPH solution were added. After a 30-minute incubation at ambient temperature in the absence of light, the final absorbance of the samples was recorded at 517 nm. Ascorbic acid and trolox were used as standards. DMSO was used as a negative control. All tests were performed in triplicate, and the results were averaged [20].

2.2.4. Anticancer and cytotoxicity studies.

The anticancer potential of the compounds was evaluated against the A549 lung cancer cell line, whereas their cytocompatibility was screened using healthy human dermal fibroblast (HDF-1) cells. A549 cells were cultured in RPMI-1640 medium supplemented with 10% Fetal Bovine Serum, 1% Penicillin/Streptomycin, and 1% L-glutamine. Conversely, DMEM medium was utilized under identical supplementation conditions for the culture of HDF-1 cells. Both cell lines were incubated at 37°C in a humidified atmosphere containing 5% CO2. Subculturing was routinely executed every few days, depending on the monolayer density. Upon reaching 70-80% confluence in T25 flasks, the cells were detached through trypsinization. Cell population densities were subsequently quantified using a Neubauer hemocytometer under an inverted microscope. For the biological treatments, the synthesized imine-metal complexes were dissolved in DMSO at concentrations of 6.25, 12.5, 25, 50, 100, and 200 µM. Following the administration of these solutions to the cells, the plates were incubated for 48 hours. For verification, each assay was carried out in triplicate. The control group was medium only, with methotrexate (MTX) as a positive control. 0.1 % DMSO was used as a negative control.

2.2.4.1. WST-8 assay for cell proliferation.

To evaluate the anticancer and cytotoxic effects of imino-metal complexes, the "Cell Proliferation Detection Kit-8 (CVDK-8)" was used [21]. For this purpose, A549 and HDF-1 cells were seeded in a 96-well plate at a density of $7x10^3$ cells per well and incubated for 24 hours to allow them to adhere to the surface. After incubation, the compounds were prepared at the specified concentrations (6.25, 12.5, 25, 50, 100, 200 µM) and applied to the cells for a 48-hour treatment. After the drug application, 50 µL of the 10% CVDK-8 solution was added to each well, and the cells were incubated at 37°C in a 5% CO_2 incubator for 4 hours. At the end of the period, the absorbance of the color formed was measured at 450 nm using a spectrophotometer. The IC_{50} values of the compounds were determined by comparing the absorbance of the drug-treated groups with that of the control group. The control group was medium only, with methotrexate as a positive control, and 0.1 % DMSO was used as a negative control.

$$Cell\ viability\ (\%) = \frac{[Abs_{(treated)} - Abs_{(WST-8cell\ free)}]}{[Abs_{(control)} - Abs_{(WST-8cell\ free)}]}\ x\ 100 \qquad (1)$$

2.2.4.2. SRB assay for cell proliferation.

The impacts of the synthesized imine-metal complexes on the total protein concentrations of HDF-1 and A549 cells were monitored using the SRB colorimetric test. Initially, a 24-hour seeding phase at 37°C in a 5% CO_2 environment was performed in 96-well plates using cells at 70-80% confluence. The cells were subsequently exposed to the IC_{50} concentrations of the complexes for 48 hours in triplicate. To fix the cell monolayer, the treatment media were removed, 100 µL of 10% ice-cold trichloroacetic acid was applied, and the plate was kept at +4°C for 1 hour. Deionized water was used to wash the wells after removing the acid solution. For the staining step, 50 µL of SRB solution was kept in the wells for 30 minutes at room temperature away from light. The residual dye was rinsed away with 1% acetic acid, and the plates were thoroughly dried. To dissolve the complexes, 200 µL of 10 mM Tris base was added, and the plates were agitated on a shaker at 150 rpm for 15 minutes. Absorbance screening was executed at 564 nm to estimate total protein quantities. Methotrexate was preferred as a standard, and medium-only wells served as the control group. as a positive control, and 0.1 % DMSO was used as a negative control [22].

$$Total\ protein\ (\%) = \frac{[Abs_{(treated)} - Abs_{(SRB\ reagent)}]}{[Abs_{(control)} - Abs_{(SRB\ reagent)}]}\ x\ 100 \qquad (2)$$

2.3. In silico and statistical analyses.

2.3.1. Molecular modeling and in silico ADME evaluations.

2.3.1.1. Preparation of proteins and ligands.

In this study, the predicted protein targets of the metal complexes were determined using the SwissTargetPrediction online software. The three-dimensional (3D) crystal structures of the identified proteins-namely Human Serum Albumin (PDB ID: 1A06), DNA polymerase (PDB ID: 1A35), Vascular Endothelial Growth Factor and Receptor (PDB ID: 3V2A), Copper Transporter 1 (PDB ID: 6M97), 5-lipoxygenase-activating protein (FLAP) (PDB ID: 2Q7R), Superoxide Dismutase (PDB ID: 8KB3), DNA Gyrase (PDB ID: 6RKS), Dihydrofolate reductase (PDB ID: 1RF7), Matrix Metalloproteinase-9 (PDB ID: 1L6J), Caspase-3 (PDB ID: 6BDV), Antioxidant 1 Copper Chaperone (PDB ID: 5F0W), Carbonic anhydrase II (PDB ID: 2VVB), and Zinc transporter proteins (PDB ID: 5TSA) were retrieved from the Protein Data Bank (PDB) database. The downloaded protein structures were processed using the Protein Preparation module in BIOVIA Discovery Studio. During this preparation process, unnecessary water molecules were removed, missing atoms and side chains were completed, appropriate protonation states were assigned, and the structures were minimized to achieve low-energy conformations. The 3D structures of the synthesized metal complexes were sketched in ChemDraw, converted to .pdb format, and subsequently optimized using AutoDockTools v.1.5.6 [23].

2.3.1.2. Binding site identification and docking studies.

The binding sites were defined based on the active regions of the selected proteins using the AutoDock Vina Grid Box tool. Subsequently, the binding potentials of the ligands within

these regions were investigated. Molecular docking results were evaluated based on binding affinity scores and detailed assessments of hydrogen bonds, metal-ion coordination, hydrophobic interactions, and π-π stacking. The resulting complexes were analyzed in detail using two-dimensional (2D) interaction diagrams [24].

2.3.1.3. In silico ADME analyses.

The pharmaceutical viability of the metal complexes was predicted using the online SwissADME software tool. Within this scope, key parameters including lipophilicity (log P), solubility (log S), intestinal permeability (Caco-2), blood-brain barrier (BBB) permeation, plasma protein binding (PPB) percentage, and potential interactions with cytochrome P450 enzymes were calculated [25].

2.4. Statistical analyses.

Data obtained from the studies were evaluated using GraphPad Prism 10.0 Software (GraphPad Software, La Jolla, CA). One-Way, Two-Way ANOVA, Dunnett test, and Unpaired t-tests were performed to calculate p-values, with $p<0.05$ considered significant.

3. Results and Discussion

3.1. Synthesis design.

The synthesis of the imine intermediate (3), a compound whose structural properties have been well documented in previous studies, was achieved by reacting benzaldehyde with 4-methoxyphenethylamine using the methodology outlined above [26,27]. The corresponding imine-metal complexes (4-5) were successfully prepared with yields spanning from 68% to 89% via the subsequent reaction of the imine with Zinc Chloride and Copper(II) Chloride Dihydrate. Figure 1 illustrates the conceptual synthesis design for these target molecules, and Figure 2 details the exact structural configurations of the synthesized compounds. Due to their significant therapeutic potential, imine-metal complexes represent a class of biologically active agents that exhibit remarkable antibacterial [16], antifungal [28], antioxidant [29], and anticancer activities [30]. Consequently, they have drawn substantial attention within the fields of bioinorganic and bioorganic chemistry. The preparation of these coordination compounds generally initiates with the formation of the core imine ligand, which is subsequently reacted with various metal salts to generate mono-, bi-, tri-, or tetra-dentate chelate complexes. [16]. However, a critical synthetic challenge often overlooked in the literature involves the water-sensitivity of the imine core during complexation. Since imine formation is a highly reversible condensation reaction, molecular sieves are strictly utilized during the initial step to systematically remove the 1 mole of generated water, shifting the equilibrium toward the product. Despite the meticulous nature of this step, conventional protocols often employ hydrated metal salts, such as Copper(II) Chloride Dihydrate, in the subsequent coordination stage. Introducing hydrated metal salts directly into a system containing such a hydrolytically sensitive ligand poses a severe risk of triggering the reverse reaction, potentially leading to the premature cleavage and degradation of the imine intermediate. The prominent highlight and methodological significance of the synthesis part of this study lie in addressing this delicate chemical nuance through an innovative procedural modification. To prevent hydrolytic cleavage of the core imine linkage, the hydrated metal salts were initially dissolved in absolute

ethanol, and their coordinated water molecules were thoroughly removed using molecular sieves before introduction into the reaction mixture. By successfully executing the coordination reaction in the presence of this pre-dehydrated metal matrix without altering or decomposing the core imine framework, this work demonstrates a robust and resilient synthetic design. This delicate balance achieved during the complexation process underscores the stability of the synthesized compounds and provides a valuable synthetic insight into the existing literature on the tolerance limits and synthetic protection of imine-based ligands against hydrated transition-metal frameworks.

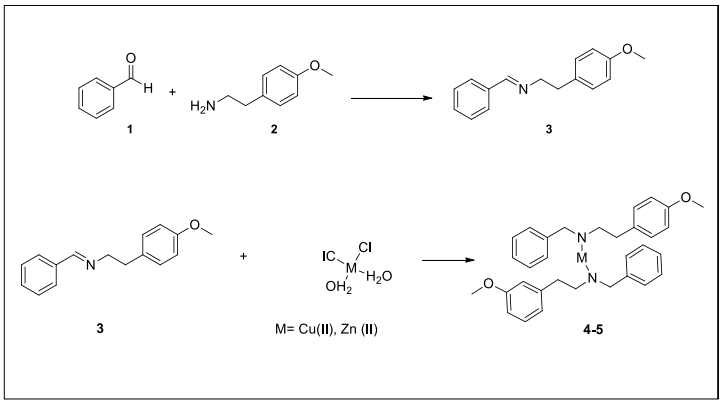

Figure 1. Schematic representation of the synthetic design, illustrating the condensation pathway for the formation of the substituted phenethylamine-based imine ligand and its subsequent coordination with copper(II) and zinc(II) metal ions using pre-dehydrated absolute ethanol.

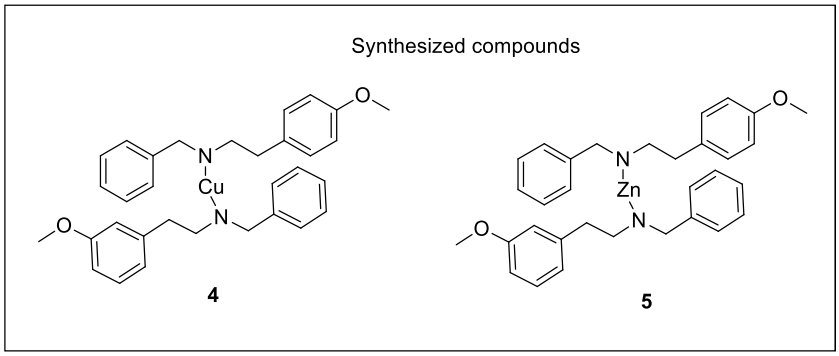

Figure 2. Proposed molecular structures and coordination geometries of the synthesized bidentate imine-metal complexes [Copper(II) complex (4) and Zinc(II) complex (5)], highlighting the coordination sites through the azomethine nitrogen and the corresponding counter-ions.

3.1.1. Structural characterization.

The core imine intermediate (3) evaluated in this work is already known in the literature [26,27]. In contrast, the newly developed imine-copper and imine-zinc metal complexes are novel. Structural confirmation of the newly synthesized imine-metal complexes (4–5) was achieved by combining FTIR, UV-Visible, mass spectrometry, and XRD analyses, with all spectral data fully supporting the anticipated chemical structures.

3.1.2. Interpretation of FTIR Spectra.

According to the collected FTIR spectra, the free imine intermediate exhibited a characteristic CH=N stretching band at 1645 cm-1. As previously reported [31], the high electronegativity of metal centers typically shifts the positions of core ligand peaks during coordination. In this study, binding to copper and zinc ions shifted the azomethine peak from

1645 cm-1 to 1595 cm-1 and 1610 cm-1, respectively. Additionally, newly developed bands corresponding to metal–nitrogen interactions were identified within the 500-600 cm-1 range, specifically demonstrating transmittance values between 530 and 551 cm-1 (Figures 3 and 4). These diagnostic spectral shifts are consistent with previous literature models [32] and firmly corroborate the successful synthesis of the target metal complexes.

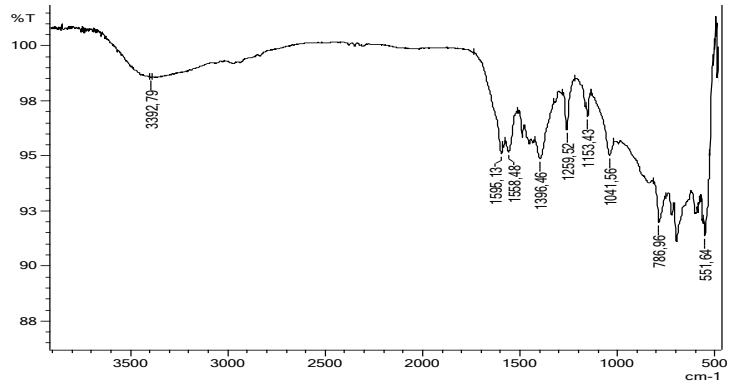

Figure 3. FTIR spectrum of the 4-methoxy phenethylamine-based imine ligand (3), confirming the successful formation of the azomethine linkage by the sharp characteristic C=N stretching vibration band observed at approximately 1645 cm^{-1}.

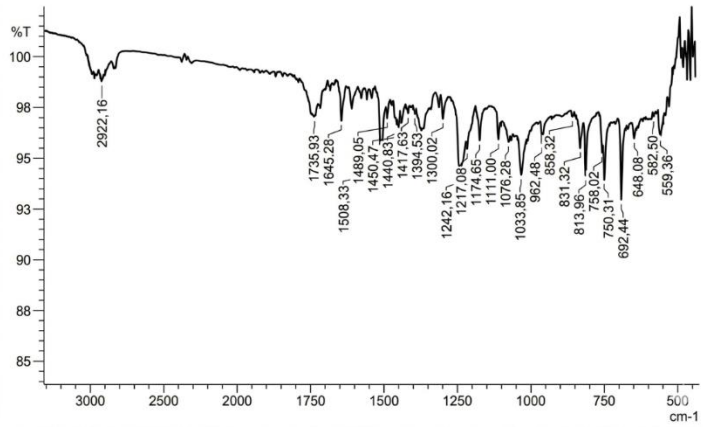

Figure 4. FTIR spectrum of the imine-copper metal complex (4), demonstrating the coordinate covalent bonding via the significant shift of the C=N band to lower frequencies (approx. 1595 cm^{-1}) and the emergence of new characteristic metal-nitrogen (M-N) stretching bands.

3.1.3. Mass spectroscopy analysis.

Mass spectrometry datasets further substantiated the structures of the prepared imine-metal complexes. For both the imine-copper (4) and imine-zinc (5) complexes, the respective molecular ion peaks were explicitly detected at 542 m/z (Figures 5 and 6). In parallel, predictive mass estimations conducted through ChemBioDraw software yielded an identical theoretical value of 542 m/z. This precise correlation between the experimental data and theoretical predictions firmly certifies the structural assignments of the coordination compounds. Additionally, the mass spectra provide detailed insights into the binding characteristics between the imine ligand and the metal centers, reinforcing the successful execution of the synthesis and the stability of the final products.

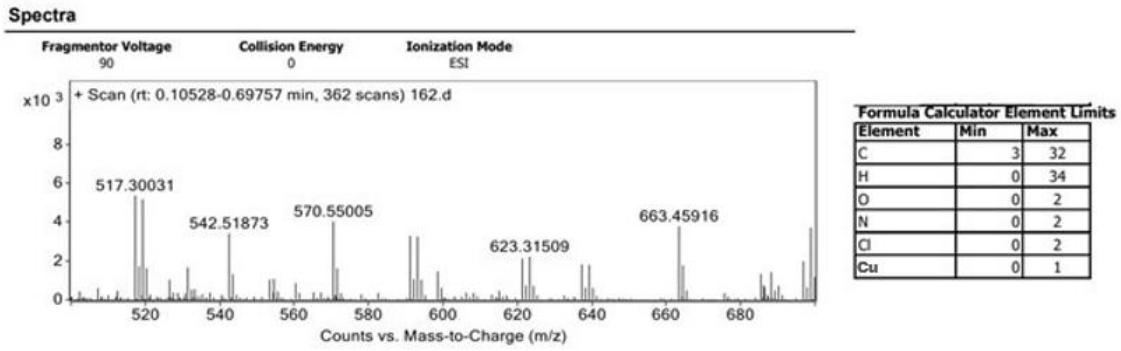

Figure 5. Mass spectrum (Q-TOF) of the Imine-Copper Complex (4), illustrating the experimental molecular ion peak $[M+H]^+$ and specific fragmentation patterns that validate the proposed stoichiometric ratio and molecular formula.

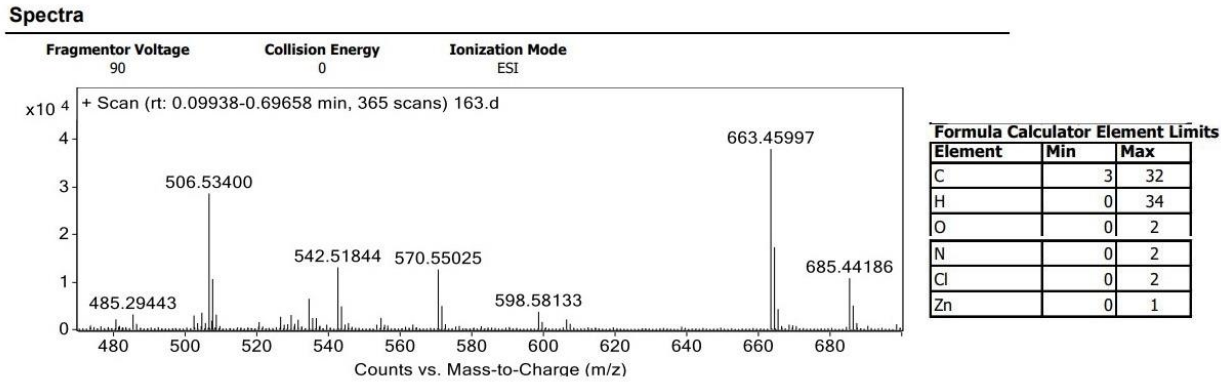

Figure 6. Mass spectrum (Q-TOF) of the Imine-Zinc Complex (5), confirming the structural integrity and purity of the complex through the identification of the primary molecular ion envelope corresponding to the theoretical isotopic distribution of Zinc.

3.1.4. XRD analysis.

The formation of crystalline phases in the prepared imine-metal complexes was successfully monitored by X-ray diffraction (Figure 7). The successful coordination between the zinc ions and imine groups was confirmed by the emergence of sharp and intense peaks in the XRD spectrum of the imine-zinc complex (5), which reflects a well-ordered crystal lattice. High crystallinity and long-range structural regularity are typical features of such sharp diffraction profiles. On the other hand, a completely different peak distribution was observed for the imine-copper complex (4), with reflections noticeably broader and less intense than those of the zinc analog. This divergence suggests that the copper complex possesses a lower structural order or exhibits amorphous tendencies. While certain scattering positions were shared with the zinc complex, the poorly defined overall copper pattern suggests an alternative, less-organized phase structure, highlighting how the specific metal center dictates variations in crystallinity and spatial organization.

To index the major diffraction peaks obtained from the XRD patterns, the lattice technique was adopted [33]. Crystallographic metrics were subsequently determined using the Scherrer formulation [34]. A comprehensive summary detailing the derived crystal dimensions, 2-theta maxima, and specific hkl planes is provided in Table 1.

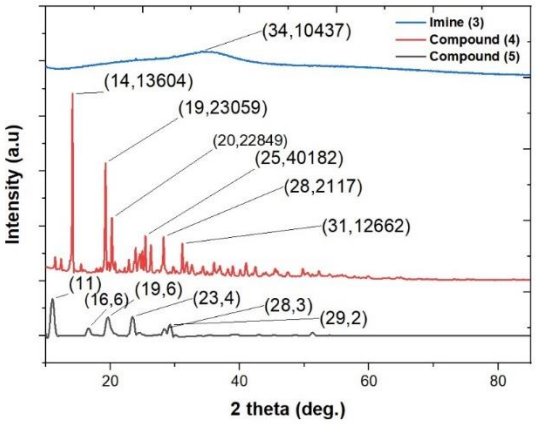

Figure 7. Powder X-ray diffraction (XRD) patterns of the synthesized Imine-Metal Complexes, comparing the high crystallinity of the Zinc complex (5) with the distinct phase distribution and structural parameters of the Copper complex (4).

Table 1. Evaluated XRD diffraction angles (2 theta), Miller indices (hkl), and calculated crystallite sizes (thickness) of the Imine-Metal Complexes derived via the Scherrer equation.

Compound	2-theta maximum	hkl indices	Crystal size
Imıne (3) Ligand	11.00724	100	16.39094856
Compound (4) Copper	14.13604	100	0.947813954
Compound (5) Zinc	34.10437	220	61.6247131

3.1.5. Coordination chemistry insights.

Coordination of the imine group—specifically the azomethine (-C=N-) functionality - with metal ions drives the formation of the target imine-metal complexes. As previously established [35,36]. This binding mechanism relies heavily on the interaction between the metal ions' electron-withdrawing nature and the imine's electron-donating properties. Variations in the spatial packing of the crystal lattice and the coordination sphere are strongly influenced by the distinct electronic configurations and geometric preferences of copper and zinc ions, accounting for the observed structural order and crystallinity. The XRD datasets not only verify that imine-metal complexation occurred but also illustrate the structural diversity triggered by altering the central metal ion. Such outcomes reinforce the versatility of imine derivatives as ligands, demonstrating their ability to form coordination complexes with highly diverse crystalline structures [37].

3.1.6. UV-vis analysis: electronic absorption spectroscopy.

The coordination behavior and electronic structures of the synthesized metal complexes (4 and 5) were investigated using UV-Vis absorption spectroscopy in DMSO solution. The corresponding electronic spectra exhibit distinct absorption bands that vary significantly depending on the nature of the metal center (Cu^{2+} vs. Zn^{2+}). In the higher-energy region (250-300 nm), both complexes exhibit intense absorption bands centered at 284 nm, with a shoulder-like transition near 227 nm. These bands are attributed to the intra-ligand π-π* and n-π* electronic transitions arising from the conjugated aromatic phenyl and methoxyphenyl rings within the ligand framework (Figure 8).

A significant divergence between the two complexes is observed above 300 nm. The Zinc complex (5) exhibits a well-defined, prominent absorption maximum (ʎmax) at approximately 350 nm. Since Zn^{2+} possesses a completely filled d^{10} electronic configuration, *d-d* transitions are quantum-mechanically forbidden; hence, this distinctive band at 350 nm is

confidently assigned to Ligand-to-Metal Charge Transfer (LMCT) or Metal-to-Ligand Charge Transfer (MLCT) transitions.

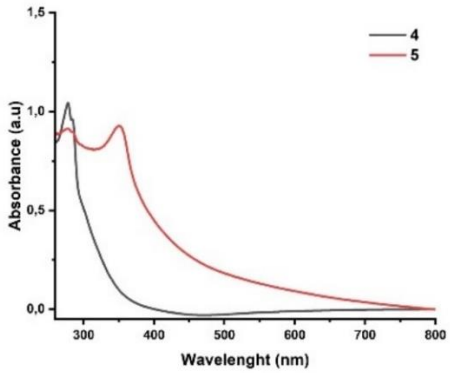

Figure 8. UV-vis electronic absorption spectra of the metal complexes recorded in solution, displaying the intra-ligand transitions (π-π* and n-π*) and the characteristic ligand-to-metal charge transfer (LMCT) bands, confirming the coordination core.

This profile indicates strong coordination between the zinc ion and the azanide/amine nitrogen donors [38]. Conversely, the Copper complex (4) shows a sharp decrease in absorbance above 300 nm, displaying no significant absorption bands in the near-UV and visible regions under the measured 500 µM concentration. The absence of noticeable *d-d* transition bands for the copper complex in the 600-800 nm region, even at this relatively high concentration level, is ascribed to the typically low molar absorptivity (Ɛ) associated with visually forbidden *d-d* transitions in certain symmetric geometric environments, which remain below the detection threshold. These spectroscopic findings confirm the successful formation of the distinct metal complexes and highlight the profound impact of the metal center on the overall electronic transition profile of the chelate structures.

3.2. Antimicrobial activity results.

To explore the antimicrobial potential of the synthesized imine-zinc and imine-copper complexes, disc diffusion assays were systematically performed against various microorganisms (Table 2). The targeted pathogens included the yeasts Candida dubliniensis and Candida albicans; the Gram-positive strains Enterococcus faecalis and Methicillin-resistant Staphylococcus aureus (MRSA); and the Gram-negative bacteria Escherichia coli and Acinetobacter baumannii. Based on the empirical data, no visible inhibition zones developed around the sample-impregnated discs, indicating that these complexes lack effective antimicrobial activity against the tested strains. This complete absence of antibacterial and antifungal activity is validated by the disc diffusion records in Table 2. Although imine-metal complexes generally exhibit promising structural advantages for bioactivity, no significant antimicrobial activity was observed in this specific trial. To uncover their latent biological value, further structural optimizations or evaluations against broader clinical strains could be considered in future studies.

Table 2. In vitro antimicrobial activity of the synthesized phenethylamine-based imine-metal complexes against selected bacterial and fungal strains evaluated by the disc diffusion method (expressed as inhibition zone diameters in mm).

Microbial Strains	**Imine-metal complex**	
	Compound (4)	**Compound (5)**
A. baumannii ATCC BAA- 1605	-	-
MRSA *ATCC 43300*	-	-

Microbial Strains	Imine-metal complex	
	Compound (4)	Compound (5)
E. coli ATCC BAA-2523	-	-
E. faecalis ATCC 49452	-	-
C. albicans ATCC 10231	-	-
C. tropicalis KÜEN 1025	-	-

The antimicrobial profile of imine-metal complexes, especially those incorporating zinc and copper centers, is highly sensitive to the precise coordination mode and ligand architecture. Although broad-spectrum antibacterial and antifungal efficiencies have been attributed to certain imine-copper structures [39], significant fluctuations in performance are common. The fact that several copper-based complexes display zero activity confirms that successful synthesis does not guarantee biomedical utility. On the other hand, even though imine-zinc compounds frequently exhibit greater toxicity than free ligands due to coordination synergy [40], examples lacking antimicrobial activity are also prevalent in the literature [41]. This structural dependency explains why the imine-copper (4) and imine-zinc (5) complexes synthesized in this study exhibited no measurable inhibition against A. baumannii, E. coli, MRSA, E. faecalis, C. albicans, and C. dubliniensis. Our results support the paradigm that antimicrobial activity is not an inherent property of imine-metal systems but is highly contingent on structural parameters. This is consistent with previous antifungal trials, in which some complexes were effective while others were not [42,43]. Therefore, the gathered evidence suggests that future research must prioritize molecular optimization and structural modifications to design effective agents against resistant clinical strains. 3.3. Antioxidant activity.

The antioxidant potentials of the synthesized metal complexes (4 and 5) were comprehensively evaluated using DPPH, ABTS radical scavenging, and CUPRAC cupric reducing antioxidant capacity assays. The concentration-dependent activity curves (Figure 9) and the calculated IC_{50} values (Table 3) were compared with those of the standard antioxidants, Ascorbic Acid and Trolox.

Table 3. The IC_{50} values (mg/mL) of the synthesized metal complexes and standard antioxidants in DPPH, ABTS, and CUPRAC assays.

	IC_{50} (mg/mL)		
Compounds/Analysis	**CUPRAC**	**DPPH**	**ABTS**
4	0.63325 ± 0.00007	0.66600 ± 0.00130	0.51738 ± 0.00137
5	0.55474 ± 0.00024	0.47508 ± 0.00088	0.59203 ± 0.00074
Ascorbic Acid	0.00941 ± 0.00064	0.01911 ± 0.00029	0.04921 ± 0.00048
Trolox	0.03363 ± 0.00037	0.03511 ± 0.00058	0.04993 ± 0.00065

IC_{50} is defined as the concentration required to inhibit or reduce 50% of the initial radical/antioxidant capacity. Data are expressed as the mean ± Standard Deviation (SD) of three independent experiments (n=3).

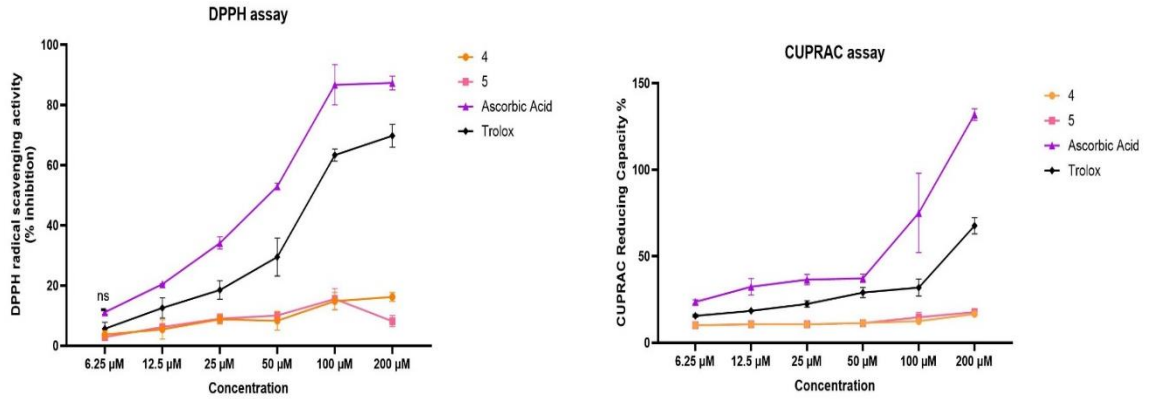

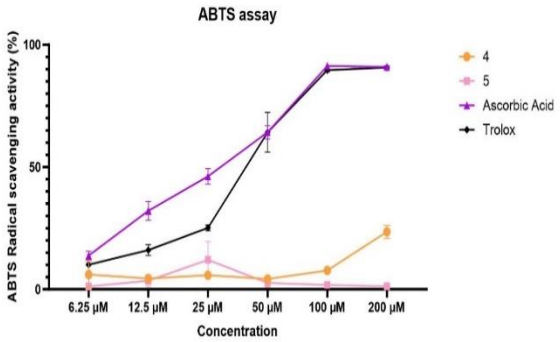

Figure 9. Antioxidant analysis results of imine-metal complexes. Two-way ANOVA confirmed significant differences ($p<0.0001$).

According to the DPPH assay results, all samples exhibited linear radical-scavenging activity with increasing concentration. The standard antioxidants, Ascorbic Acid (IC_{50}: 0.01911 mg/mL) and Trolox (IC_{50}:0.03511 mg/mL), displayed the highest inhibition at the lowest concentrations. When the synthesized metal complexes were compared, Compound 5 (IC_{50}:0.47508 mg/mL) demonstrated a significantly stronger radical scavenging performance than Compound 4 (IC_{50}:0.66600 mg/mL).

Based on the ABTS assay results, the reference agents Ascorbic Acid (IC_{50}: 0.04921 mg/mL) and Trolox (IC50: 0.04993 mg/mL) showed strong inhibition, with a sharp increase above the 50 µM threshold. Regarding the complexes' behavior against the ABTS cation, Compound 4 (IC50: 0.51738 mg/mL) was more active than Compound 5 (IC_{50}: 0.59203 mg/mL).

In the CUPRAC method, the reducing capacities of all samples increased linearly with increasing concentrations. Ascorbic Acid (IC_{50}: 0.00941 mg/mL) and Trolox (IC_{50}: 0.03363 mg/mL) exhibited a highly dynamic profile in terms of donating electrons to the system. In the evaluation among the synthesized new metal complexes, Compound 5 (IC_{50}: 0.55474 mg/mL) recorded a superior reducing potential compared to Compound 4 (IC_{50}: 0.63325 mg/mL).

The collective evaluation of the antioxidant assays indicates that the synthesized complexes exhibit a moderate-to-good antioxidant profile, consistent with the ranges reported in the literature for similar coordination compounds, although not as high as those of the reference standards. The obtained activity levels indicate that these compounds have the potential to serve as candidate protective agents against oxidative stress. Owing to their prospective biomedical and therapeutic utility, the significant antioxidant properties of transition-metal imine complexes have been well documented [6]. A prominent trend observed across various studies is the enhancement of radical-trapping capabilities upon complexation, enabling these compounds to outperform their free ligands. This antioxidant behavior is commonly reported to be dose-dependent, consistently surpassing the efficiency of the core organic molecules. However, a general consensus in the literature indicates that these coordination derivatives still fall short of the high antioxidant thresholds set by standard control agents, such as ascorbic acid. Complex relationships between chemical design and biological performance have been revealed through thorough investigations of the antioxidant profiles of imine copper-zinc complexes [44].

It is widely observed that zinc(II) and copper(II) complexes exhibit substantial antioxidant activity, often surpassing their core organic ligands but remaining less potent than conventional antioxidants such as ascorbic acid. According to previous data, these transition-metal complexes exhibit a clear dose-dependent capacity to scavenge free radicals, including

hydroxyl and DPPH radicals [45]. Nevertheless, an exception to these general literature trends was observed in the current study, where the newly synthesized metal complexes (4-5) demonstrated no detectable antioxidant activity compared with the standard references trolox and ascorbic acid.

3.4. Effects of imine-metal complexes on cell viability: analysis of WST-8 and SRB assays.

To determine the anticancer effects of the synthesized imine-metal complexes (Compounds 4-5) on A549 cells and the cytotoxic effects on HDF-1 cells, cells were treated with increasing concentrations (6.25-200 µM) of the compounds for 48 hours, and the WST-8 assay was performed. The obtained results are shown in Figures 10 and 11. On A549 cells, compound (4) (IC_{50}: 42.27 ± 0.68) ($p>0.05$, $p<0.05$, $p<0.001$) and compound (5) (IC_{50}: 45.21 ± 0.34) ($p<0.05$, $p<0.01$, $p<0.001$) were found to exhibit anticancer activity at high concentrations (50-200 µM), reducing cell viability below 50% compared to the control group. However, it has been shown that MTX (IC_{50}: 41.06 ± 0.75) ($p>0.05$, $p<0.001$) used as a positive control, also exhibited anticancer activity at high concentrations (50-200 µM), reducing cell viability below 50%. The anticancer activities of compounds (4) and (5) were similar to the positive control MTX, showing activity over a similar concentration range (50-200 µM) and close IC_{50} values (Figure 10).

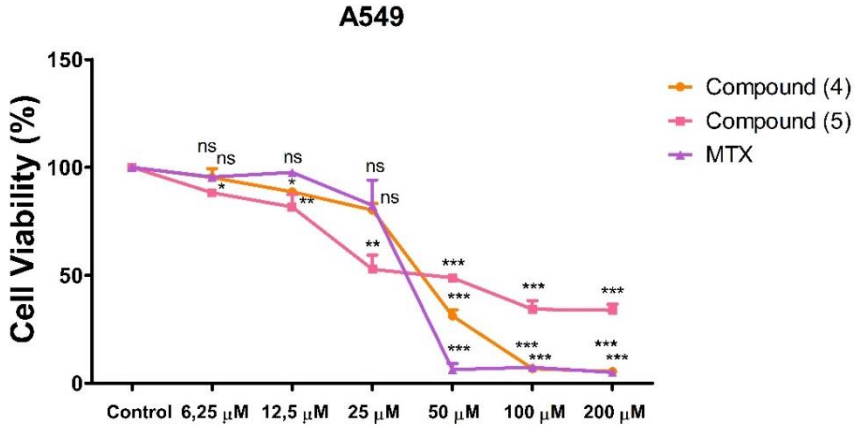

Figure 10. Anticancer activities of synthesized imine-metal complexes on the A549 cell line (ns:$p>0.05$, *$p<0.05$, **$p<0.01$, ***$p<0.001$).

In HDF-1 cells that were treated to determine the cytotoxic effects of synthesized imine-metal complexes on a healthy cell line, compound (4) (IC_{50}: 167.13 ± 0.15) ($p>0.05$, $p<0.05$, $p<0.001$) showed a significant cytotoxic effect at a high concentration (200 µM), reducing cell viability to below 50%. Compound (5) (IC_{50}: 5.09 ± 0.03) ($p<0.001$) showed a significant cytotoxic effect at all applied concentrations (6.25-200 µM), reducing cell viability to below 50%. It was determined that MTX (IC_{50}: 138.32 ± 0.23), used as a positive control ($p>0.05$, $p<0.05$, $p<0.001$), showed cytotoxicity at high concentrations (200 µM), reducing cell viability to below 50%. When the cytotoxic effects of compound (4) and compound (5) were compared with the positive control MTX, it was determined that compound (4) had less cytotoxic effect than MTX, while compound (5) had a higher cytotoxic effect than MTX. The selectivity indices of the compounds were calculated, and it was determined that compound (4) has a selectivity index of 3.95 and compound (5) has a selectivity index of 0.11. Considering the results, compound (4) shows good selectivity, as it is more effective in A549 cells and less toxic in HDF-1 cells. However, compound (5) shows poor selectivity, as its toxicity in HDF-1 cells is higher than in A549 cells (Figure 11).

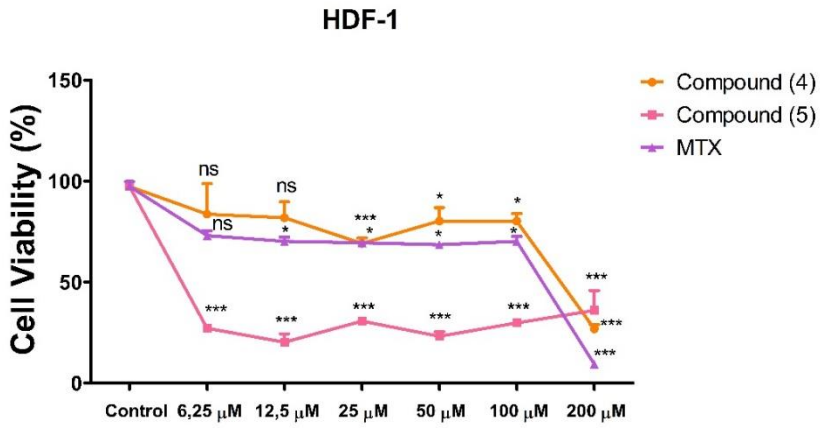

Figure 11. Cytotoxic effects of synthesized imine-metal complexes on HDF-1 cell line (ns: $p>0.05$, *$p<0.05$, ***$p<0.001$).

To determine the effect of the synthesized Imine-metal complexes on the total protein amount of A549 cells, the IC_{50} concentrations of compound (4) and compound (5) determined by the WST-8 test were applied for 48 hours. In cells treated with compound (4) (IC_{50}: 42.27 µM), the total protein amount was found to be 56% ($p<0.01$), while in cells treated with compound (5) (IC_{50}: 45.21 µM), the total protein amount was found to be 63% ($p<0.05$). It has been shown that the total protein amount of cells treated with MTX (IC_{50}: 41.06 µM) as a positive control was 37% ($p<0.001$). When the total protein amounts of compound (4) and compound (5) were compared with the positive control MTX, it was shown that MTX caused a greater reduction in total protein amounts than both compounds (Figure 12).

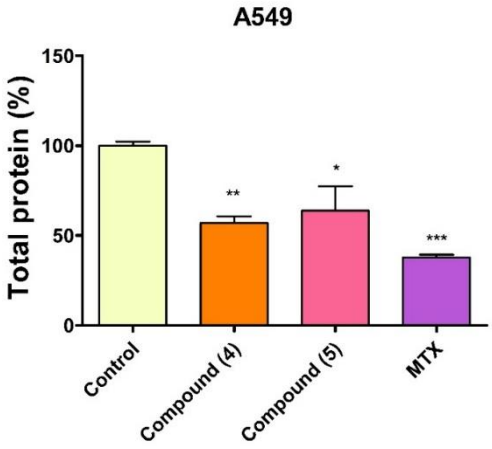

Figure 12. Effects of synthesized Imine-metal complexes on the total protein amount of A549 cells (*$p<0.05$, **$p<0.01$, ***$p<0.001$).

To determine the effects of the synthesized imine-metal complexes on the total protein amount of HDF-1 cells at the IC_{50} concentrations identified in A549 cells, compound (4) (42.27 µM) and compound (5) (45.21 µM) were applied. In cells treated with compound (4), the total protein amount was 94% ($p>0.05$); in cells treated with compound (5), the total protein amount was 11% ($p<0.001$). In cells treated with MTX (41.06 µM) as a positive control, total protein levels were 49% higher ($p<0.001$). When the total protein amounts of compound (4) and compound (5) were compared with the positive control MTX, it was shown that MTX caused a greater reduction in total protein amount than compound 4, while compound 5 caused a greater reduction in total protein amount than MTX. Due to the compound 5's high cytotoxicity, a significant decrease in total protein levels was also observed (Figure 13).

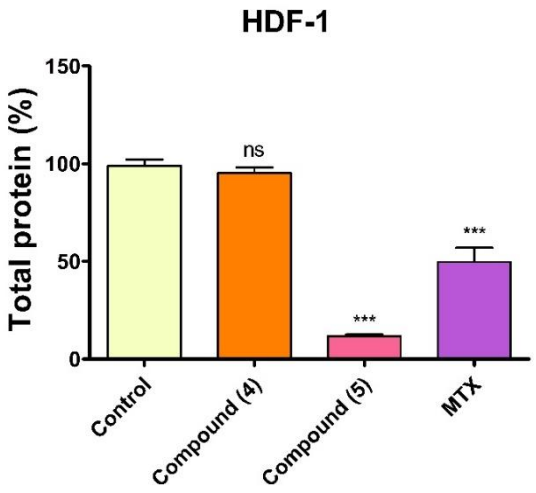

Figure 13. Effects of synthesized imine-metal complexes on the total protein amount of HDF-1 cells (ns: $p>0.05$, ***$p<0.001$).

Considerable scientific interest has been focused on the anticancer efficacy of imine-metal complexes, driven by their unique biological behaviors. The potent tumor-inhibiting profiles of various imine-based metal derivatives against cancer cell lines have been documented in recent literature. Investigation of these compounds in the A549 lung cancer model highlights their viability for oncology applications [46]. According to Gomes et al. (2024), imine-copper complexes can screen and eliminate malignant cells with efficiencies that often eclipse those of conventional agents such as cisplatin [47]. Cell death pathways are readily activated by copper complexes coordinated with imine ligands, yielding promising outcomes in A549 lung cancer cells [48]. A study by Gul et al. further established that imine-copper systems exert their anticancer effects by intercepting autophagy and apoptosis routes in the A549 cell line. These findings are highly consistent with the dose-dependent anticancer activity of the imine-copper complex against A549 cells observed in our current analysis [49]. Nevertheless, the newly developed imine-copper complexes also manifested a dose-dependent cytotoxicity toward healthy HDF cells. The enhanced cytotoxicity of such copper derivatives is frequently attributed to their strong DNA-binding properties, a trait that is typically enhanced in diimine-copper architectures evaluated across different tumor models. Since the imine-copper complex synthesized in this work features a distinctive diimine scaffold, its biological performance and cellular interactions are well supported by these literature models [50].

Owing to their potential to offer enhanced therapeutic outcomes with reduced systemic toxicities compared to classical treatments, imine and zinc-based metal complexes have garnered significant attention. The ability of these coordination compounds to interact with DNA and exert cytotoxic effects across a wide spectrum of cancer cell lines is well supported by the literature. In particular, increased DNA intercalation capacity has been documented for zinc(II) diimine complexes, significantly amplifying their cytotoxicity against malignant cells [51]. This critical DNA-binding affinity is especially pronounced in complexes featuring cobalt, zinc, and imine ligands, serving as the primary mechanism underlying their documented anticancer activities [52]. Zinc complexes have been shown to exhibit better selectivity and efficacy than traditional platinum-based drugs, suggesting their potential as safer alternatives [51]. In this study, imine-copper and imine-zinc complexes showed dose-dependent anticancer activity against the A549 cancer cell line, consistent with the literature. Compound (4) (3.95)

was found to have a better selectivity index, while compound (5) (0.11) was found to have a poor selectivity index.

3.5. Result of in silico analysis.

To elucidate the molecular mechanisms underlying the in vitro antiproliferative, antimicrobial, and antioxidant profiles of the synthesized Schiff base metal complexes (4-5), in-silico molecular docking simulations were performed against 13 key therapeutic protein targets. Both complexes exhibited robust binding affinities ranging from -7.0 to -10.2 kcal/mol, indicating highly specific conformational and molecular fitting within the designated receptor pockets rather than nonspecific interactions Table 4.

Table 4. Computed molecular docking parameters, including the lowest binding affinity energies (kcal/mol), imine-metal complexes within the active binding pockets of the target receptor proteins.

Protein/PDB ID	Binding Affinity Energy (kcal/mol)	
	Metal Complex	
	4	**5**
Human Serum Albumin (PDB ID: 1A06)	-8.0	-8.6
DNA polymerase (PDB ID: 1A35)	-7.0	-7.3
VEGFR (PDB ID: 3V2A)	-7.2	-7.0
Carbonic anhydrase II (PDB ID: 2VVB)	-7.7	-8.0
FLAP (PDB ID: 2Q7R)	-8.0	-10.1
Superoxide Dismutase (PDB ID: 8KB3)	-8.7	-8.9
DNA Gyrase (PDB ID: 6RKS)	-8.2	-7.4
Dihydrofolate reductase (PDB ID: 1RF7)	-10.2	-8.7
Metalloproteinase Matrix-9 (PDB ID: 1L6J)	-9.0	-7.9
Caspase-3 (PDB ID: 6BDV)	-7.9	-8.2
Antioxidant 1 Copper Chaperone (PDB ID: 5F0W)	-6.7	-
Copper Transporter 1 (PDB ID: 6M97)	-8.0	-
Zinc transporter proteins (PDB ID:5TSA)	-	-7.7

Antibacterial mechanisms of action were investigated using bacterial nucleic acid replication enzymes, namely DHFR and DNA Gyrase. Complex 4 exhibited the most dominant interaction with DHFR among the entire study, with a binding energy of -10.2 kcal/mol (Figure 10), while significantly outperforming complex 5 on DNA Gyrase (-8.2 to -7.4 kcal/mol).

To substantiate the in vitro radical scavenging activity, docking was performed against Superoxide Dismutase (SOD). Both complexes 4 and 5 demonstrated exceptionally strong and comparable binding energies (-8.7 and -8.9 kcal/mol, respectively). The extensive hydrogen bonding and hydrophobic networks established by the Schiff base ligand architecture within the SOD catalytic site theoretically support the compounds' capacity to mitigate cellular oxidative stress, highlighting their prominent SOD-mimetic potential.

The evaluation of cytotoxicity pathways focused on angiogenic and apoptotic cascades via VEGFR, MMP-9, FLAP, and Caspase-3. In the tumor microenvironment matrix, complex 4 displayed a superior binding affinity of -9.0 kcal/mol toward MMP-9 compared to complex 5 (-7.9 kcal/mol), suggesting its enhanced potential to suppress cancer cell invasion and metastasis. Conversely, complex 5 achieved a remarkable docking score of -10.1 kcal/mol against FLAP, a crucial enzyme in inflammation-driven oncogenesis, corroborating the initial SwissTargetPrediction nuclear receptor affinity. Crucially, the high affinities observed for both compounds toward Caspase-3 (-7.9 and -8.2 kcal/mol, respectively) provide theoretical validation that their cytotoxicity is driven by apoptosis rather than necrosis.

An integrative evaluation combining pharmacokinetic profiles with pharmacodynamic data reveals a strong correlation between systemic transport boundaries and molecular target preferences: Hydrophobicity vs. Plasma Transport. SwissADME screening predicted high lipophilicity (Consensus Log P ~5.39) and a "Poorly Soluble" profile for both derivatives. This systemic solubility barrier is overcome by the docking data, which show that both complexes display high affinity for Human Serum Albumin (HSA) (-8.0 and -8.6 kcal/mol). This confirms that the complexes safely overcome the aqueous solubility limit by binding stably to plasma albumin for systemic distribution. Passive Absorption vs. Metal-Specific Active Transport: While structural bulkiness limited passive gastrointestinal and low-GI absorption, docking revealed distinct active-transport capabilities. Complex 4 utilized copper homeostatic routes, binding strongly to CTR1 (-8.0 kcal/mol) and ATOX1 (-6.7 kcal/mol), enabling active cellular entry and copper-induced pro-oxidant cytotoxicity in cancer cells overexpressing CTR1 and ATOX1. Conversely, complex 5 selectively bound to ZnT transporters (-7.7 kcal/mol). Combined with its affinity for zinc finger motifs, this establishes that the Zn(II) complex exerts its therapeutic effect primarily by modulating gene expression and disrupting zinc homeostasis rather than by direct nucleic acid damage.

When molecular docking studies and in vitro biological activity results are evaluated together, remarkable mechanistic correlations are observed between the target affinities and the cellular responses of the imine-metal complexes (Compound 4 and Compound 5). Although Compound 4 exhibits the highest binding affinity against DNA Gyrase (PDB ID: 6RKS, -8.2 kcal/mol) and Dihydrofolate Reductase (DHFR, PDB ID: 1RF7, -10.2 kcal/mol) enzymes, which play critical roles in bacterial replication and folate biosynthesis in molecular docking simulations, this situation is not reflected in the in vitro antimicrobial activity in the disc diffusion assay (no zone formation is observed); this paradoxical phenomenon is attributed to the inability of the complexes to diffuse into the cell through the bacterial peptidoglycan cell wall or the outer membrane porins of Gram-negative bacteria (permeability barrier), contrasting with their high enzyme inhibition potential at the molecular level. On the other hand, the theoretical superiority demonstrated by Compound 4 against VEGFR (PDB ID: 3V2A, -7.2 kcal/mol) and Matrix Metalloproteinase-9 (MMP-9, PDB ID: 1L6J, -9.0 kcal/mol) proteins, which play key roles in tumor angiogenesis and metastasis processes, is in perfect agreement with the in vitro anticancer data; indeed, Compound 4 triggers a powerful cytotoxicity and a total protein decrease that competes with the positive control MTX by dramatically reducing cell viability to around 25% at concentrations of 50 µM and above in the A549 lung cancer cell line. The most critical finding emerges in the selectivity of the compounds on healthy tissues; Compound 5 exhibits a non-specific, uncontrolled cellular toxicity that reduces healthy HDF-1 fibroblast cell viability to the 25% threshold even at the lowest dose (6.25 µM) by showing high affinity to Caspase-3 (PDB ID: 6BDV, -8.2 kcal/mol), the executor of the apoptotic signaling pathway, and inflammatory FLAP (PDB ID: 2Q7R, -10.1 kcal/mol) proteins. In contrast, Compound 4 maintains healthy HDF-1 cell viability at around 80% up to 100 µM and does not disrupt total protein synthesis, thereby demonstrating high tumor selectivity and a safe biocompatibility profile. In antioxidant analyses, the theoretical strong interaction of both compounds with the Superoxide Dismutase (SOD, PDB ID: 8KB3) enzyme is supported by the experimental data; while Compound 5 stands out relatively with lower IC_{50} values in CUPRAC IC_{50}: 0.55474 mg/mL for Compound 5, IC_{50}: 0.63325 mg/mL for Compound 4) and DPPH (IC_{50}: 0.47508 mg/mL for Compound 5, IC_{50}: 0.66600 mg/mL for Compound 4) assays, Compound 4 draws a more active profile in the

ABTS radical scavenging assay (IC_{50}: 0.51738 mg/mL), proving that its electron-donating and free radical-trapping capability varies depending on the medium.

4. Conclusions

In this study, a substituted phenethylamine-based imine ligand, (*E)-N-benzylidene-2-(4-methoxyphenethyl)ethanamine*, and its novel Cu (II) and Zn (II) metal complexes were successfully synthesized and characterized using FTIR, UV-Visible, mass spectrometry, and XRD analyses. The structural characterization confirmed the successful coordination of the imine nitrogen to the metal centers, with XRD data revealing a higher degree of crystallinity for the zinc complex than for the copper complex, which is more amorphous. The biological evaluation of these complexes yielded the following key findings.

Both imine-metal complexes showed moderate anticancer activity in A549 cells, with the IC_{50} value of the Cu complex being 42.27 ± 0.68 µM and the IC_{50} value of the Zn complex being 45.21 ± 0.34 µM. SRB analysis revealed that the total protein content in A549 cells was 56% for the Cu complex and 63% for the Zn complex. The Cu complex showed cytotoxic effects at high concentrations in HDF-1 cells (IC_{50}: 167.13 ± 0.15 µM), while the Zn complex showed high cytotoxic effects at all tested concentrations (6.25-200 µM) (IC_{50}: 5.09 ± 0.03 µM). SRB analysis revealed cytotoxicity levels of 94% and 11% in HDF-1 cells, respectively. While these complexes moderately targeted cancer cells, HDF-1 cells also showed dose-dependent cytotoxicity. Compound (4) (3.95) was found to have a better selectivity index, while compound (5) (0.11) was found to have a poor selectivity index. Under the specific experimental conditions and concentrations tested, the complexes did not show any inhibitory effects against the selected bacterial and fungal pathogens. In this study, the antioxidant potentials of the newly synthesized metal complexes (4 and 5) were successfully evaluated using DPPH, ABTS, and CUPRAC assays. Both complexes exhibited stable, concentration-dependent radical-scavenging and cupric-reducing capacities. Although the compounds were not as active as the reference standards (Ascorbic Acid and Trolox), they recorded a moderate-to-good antioxidant profile consistent with the literature. Among the tests, Compound 5 was superior in the DPPH and CUPRAC assays, whereas Compound 4 showed better performance in scavenging the ABTS cation. In conclusion, these coordination compounds possess the potential to be evaluated in future advanced biological studies as novel antioxidant candidates against oxidative stress-induced damage. In molecular docking studies, the binding mechanism of the synthesized Schiff base complexes (4-5) was evaluated. The Cu(II) complex (4) showed superior thermodynamic stability and molecular fit over the Zn(II) complex. The most dominant interaction was between the Cu-complex and bacterial DHFR (-10.2 kcal/mol), while both complexes exhibited strong affinities (>-9.0 kcal/mol) for VEGFR, MMP-9, and FLAP, demonstrating that the metal center determines binding affinity. Overall, theoretical and experimental data highlight Compound 4 as a promising chemotherapeutic agent, with potent and selective cytotoxicity against lung cancer cells, safety toward healthy tissues, and antioxidant protective capacity.

In conclusion, the newly synthesized imine-metal complexes demonstrate promising antioxidant capacities and targeted efficacy against lung cancer cells, making them compelling candidates for future oncological research despite lacking broad-spectrum antimicrobial activity. Future studies should focus on structural modifications to further optimize the selectivity index of the copper (II) complex, reduce the high toxicity of the zinc (II) derivative, and investigate underlying molecular pathways, such as apoptosis. Supported by *in silico*

docking data revealing exceptional affinity toward critical target enzymes, these theoretical and experimental findings significantly contribute to the strategic design of metal-based therapeutic agents in bioinorganic chemistry.

Author Contributions

Formal analysis, T.Y.B., M.Y., and E.A.; writing—original draft preparation, T.Y.B., M.Y., and E.A.; writing—review and editing, T.Y.B., M.Y., E.A., A.G., and B.O.; supervision, A.G. and B.O. All authors have read and agreed to the published version of the manuscript.

Institutional Review Board Statement

Not applicable.

Informed Consent Statement

Not applicable.

Data Availability Statement

All data generated or analyzed during this study are included in this published article.

Funding

This research received no external funding.

Acknowledgments

This study was supported by TUBITAK-2209-A University Students Research Projects Support Program (2022/02). We want to thank TUBITAK for their financial support and research conditions.

Conflicts of Interest

The authors declare no conflict of interest.

References

1. Raczuk, E.; Dmochowska, B.; Samaszko-Fiertek, J.; Madaj, J. Different Schiff Bases—Structure, Importance and Classification. *Molecules* **2022**, *27*, 787, https://doi.org/10.3390/molecules27030787.
2. Song, Y.; Fan, L.; Duan, S.; Tang, Z.; Liu, W.; Ansari, K.R.; Singh, A.; Lin, Y.; Talha, M. Role of C═C Double Bond in Improving the Protective Film Properties of Schiff-Base Inhibitors on N80 Steel: An Integrated Experimental and Theoretical Study. *Langmuir* **2026**, *42*, 14835-14856, https://doi.org/10.1021/acs.langmuir.6c00772.
3. Zhang, Z.; Song, Q.; Jin, Y.; Feng, Y.; Li, J.; Zhang, K. Advances in Schiff Base and Its Coating on Metal Biomaterials—A Review. *Metals* **2023**, *13*, 386, https://doi.org/10.3390/met13020386.
4. Ceyhan, G.; Köse, M.; Tümer, M.; Demirtaş, İ.; Şahin Yağlioğlu, A.; McKee, V. Structural characterization of some Schiff base compounds: Investigation of their electrochemical, photoluminescence, thermal and anticancer activity properties. *J. Lumin.* **2013**, *143*, 623-634, https://doi.org/10.1016/j.jlumin.2013.06.002.
5. Hameed, A.; al-Rashida, M.; Uroos, M.; Abid Ali, S.; Khan, K.M. Schiff bases in medicinal chemistry: a patent review (2010-2015). *Expert Opin. Ther. Pat.* **2017**, *27*, 63-79, https://doi.org/10.1080/13543776.2017.1252752.

6. Ibrahim, M.; Nabi, H.U.; Muhammad, N.; Ikram, M.; Khan, M.; Ibrahim, M.; AlAsmari, A.F.; Alharbi, M.; Alshammari, A. Synthesis, Antioxidant, Molecular Docking and DNA Interaction Studies of Metal-Based Imine Derivatives. *Molecules* **2023**, *28*, 5926, https://doi.org/10.3390/molecules28155926.
7. Jafari, M.; Salehi, M.; Kubicki, M.; Arab, A.; Khaleghian, A. DFT studies and antioxidant activity of Schiff base metal complexes of 2-aminopyridine. Crystal structures of cobalt(II) and zinc(II) complexes. *Inorg. Chim. Acta* **2017**, *462*, 329-335, https://doi.org/10.1016/j.ica.2017.04.007.
8. Göycincik, S.; Danahaliloğlu, H. Antioxidant and Antibacterial Activities of Salen-type Schiff Base and Metal Complexes. *Bitlis Eren Üniversitesi Fen Bilimleri Dergisi* **2023**, *12*, 329–336, https://doi.org/10.17798/bitlisfen.1185118.
9. Kostova, I.; Saso, L. Advances in Research of Schiff-Base Metal Complexes as Potent Antioxidants. *Curr. Med. Chem.* **2013**, *20*, 4609–4632, https://doi.org/10.2174/09298673113209990149.
10. Kumar, R.; Singh, A.A.; Kumar, U.; Jain, P.; Sharma, A.K.; Kant, C.; Haque Faizi, M.S. Recent advances in synthesis of heterocyclic Schiff base transition metal complexes and their antimicrobial activities especially antibacterial and antifungal. *J. Mol. Struct.* **2023**, *1294*, 136346, https://doi.org/10.1016/j.molstruc.2023.136346.
11. Juliana, J.; Kristiane Fanti Del Pino, S.; Fernanda, T.; Rafael Rodrigo Piva, V.; Osmar Ignacio Ayala, C.; Isis Juliane Arantes, G.; David Monteiro de, S.; Tiago Elias Allievi, F.; Giancarlo Di Vaccari, B.; Antonio Luiz, B.; Sumbal, S.; Haroon ur, R.; Jamal, R. Recent Advances on the Antimicrobial Activities of Schiff Bases and their Metal Complexes: An Updated Overview. *Curr. Med. Chem.* **2024**, *31*, 2330-2344, https://doi.org/10.2174/0929867330666230224092830.
12. Lv, L.; Zheng, T.; Tang, L.; Wang, Z.; Liu, W. Recent advances of Schiff base metal complexes as potential anticancer agents. *Coord. Chem. Rev.* **2025**, *525*, 216327, https://doi.org/10.1016/j.ccr.2024.216327.
13. Tadele, K.T.; Tsega, T.W. Schiff Bases and their Metal Complexes as Potential Anticancer Candidates: A Review of Recent Works. *Anticancer Agents Med. Chem.* **2019**, *19*, 1786–1795, https://doi.org/10.2174/1871520619666190227171716.
14. Ghosh, D.; Das, T.; Karmakar, S.; Bhar, S.; Kar, K.; Mondal, S.; Zangrando, E.; Das, D.; Chandra, A. A mechanistic insight into the anticancer activity of two novel metal Schiff base complexes through spectrophotometric and computational approach against melanoma. *Inorg. Chem. Commun.* **2026**, *184*, 116001, https://doi.org/10.1016/j.inoche.2025.116001.
15. Genç, H.; Kalin, R.; Köksal, Z.; Sadeghian, N.; Kocyigit, U.M.; Zengin, M.; Gülçin, İ.; Özdemir, H. Discovery of Potent Carbonic Anhydrase and Acetylcholinesterase Inhibitors: 2-Aminoindan β-Lactam Derivatives. *Int. J. Mol. Sci.* **2016**, *17*, 1736, https://doi.org/10.3390/ijms17101736.
16. Singh, K.; Siwach, P. Synthesis, spectroscopic, theoretical and biological evaluation of novel Schiff base complexes of divalent transition metals. *Appl. Organomet. Chem.* **2022**, *36*, e6553, https://doi.org/10.1002/aoc.6553.
17. Özgeriş, F.B.; Kaci, F.N.; Özgeriş, B.; Görmez, A. The Synthesis of Unsymmetrical Urea from Substituted Phenethylamine and the Investigation of its Antibacterial, Anticancer, and Antioxidant Properties. *Biointerface Res. Appl. Chem.* **2022**, *12*, 7052–7063, https://doi.org/10.33263/BRIAC125.70527063.
18. Aksu, K.; Özgeriş, B.; Taslimi, P.; Naderi, A.; Gülçin, İ.; Göksu, S. Antioxidant Activity, Acetylcholinesterase, and Carbonic Anhydrase Inhibitory Properties of Novel Ureas Derived from Phenethylamines. *Arch. Pharm. Chem. Life Sci.* **2016**, *349*, 944-954, https://doi.org/10.1002/ardp.201600183.
19. Gülçin, I. Measurement of antioxidant ability of melatonin and serotonin by the DMPD and CUPRAC methods as trolox equivalent. *J. Enzyme Inhib. Med. Chem.* **2008**, *23*, 871–876, https://doi.org/10.1080/14756360701626223.
20. Tohma, H.S.; Gulçin, I. Antioxidant and Radical Scavenging Activity of Aerial Parts and Roots of Turkish Liquorice (*Glycyrrhiza Glabra* L.). *Int. J. Food Prop.* **2010**, *13*, 657–671, https://doi.org/10.1080/10942911003773916.
21. Kucuk, A.; Caglar, H.O.; Karatas, O.F.; Biray Avci, C.; Gunduz, C. In vitro assessment of siRNA-mediated LRP5 silencing and temozolomide treatment in glioblastoma and brain cancer stem cells. *Mol. Genet. Genomics* **2026**, *301*, 33, https://doi.org/10.1007/s00438-026-02357-8.
22. Savale, S.K. Sulforhodamine B (SRB) Assay Of Curcumin Loaded Nanoemulsion By Using Glioblastoma Cell Line. *Asian J. Biomater. Res.* **2017**, *3*, 26–30.

23. Trott, O.; Olson, A.J. AutoDock Vina: Improving the speed and accuracy of docking with a new scoring function, efficient optimization, and multithreading. *J. Comput. Chem.* **2010**, *31*, 455–461, https://doi.org/10.1002/jcc.21334.
24. C, S.; S, D.K.; Ragunathan, V.; Tiwari, P.; A, S.; P, B.D. Molecular docking, validation, dynamics simulations, and pharmacokinetic prediction of natural compounds against the SARS-CoV-2 main-protease. *J. Biomol. Struct. Dyn.* **2022**, *40*, 585-611, https://doi.org/10.1080/07391102.2020.1815584.
25. Daina, A.; Michielin, O.; Zoete, V. SwissADME: a free web tool to evaluate pharmacokinetics, drug-likeness and medicinal chemistry friendliness of small molecules. *Sci. Rep.* **2017**, *7*, 42717, https://doi.org/10.1038/srep42717.
26. Yildirim, M.; Ozgeris, B.; Gormez, A. Substituted phenethylamine-based β-lactam derivatives: Antimicrobial, anticancer, and β-lactamase inhibitory properties. *Bioorg. Chem.* **2022**, *129*, 106212, https://doi.org/10.1016/j.bioorg.2022.106212.
27. Sidhu, A.; Sharma, J.R.; Rai, M. ChemInform Abstract: Chemoselective Reaction of Malononitrile with Imine-ones and Antifungal Potential of Products. *ChemInform* **2010**, *41*, https://doi.org/10.1002/chin.201024075.
28. El-Baradie, K.; El-Sayed, Y.S.; El-Wakiel, N.; Salem, B.M.; El-Nagar, A. Novel indazole Schiff base metal chelates as potential antifungal agents: synthesis, characterization, and computational analysis. *Chem. Biol. Technol. Agric.* **2025**, *12*, 58, https://doi.org/10.1186/s40538-025-00769-z.
29. Turan, N.; Kızılkaya, S.; Buldurun, K.; Çolak, N.; Akdeniz, A.; Bursal, E. Synthesis, enzyme inhibitory and antioxidant activities, and molecular docking studies of metal complexes of a Schiff base ligand bearing pyridine moiety. *J. Mol. Struct.* **2025**, *1338*, 142167, https://doi.org/10.1016/j.molstruc.2025.142167.
30. Bufarwa, Saleh M.; Belaidi, M.; Abbass, Leila M.; Thbayh, Dalal K. Anticancer Activity, DFT, Molecular Docking, ADMET, and Molecular Dynamics Simulations Investigations of Schiff Base Derived From 2,3-Diaminophenazine and Its Metal Complexes. *Appl. Organomet. Chem.* **2025**, *39*, e7953, https://doi.org/10.1002/aoc.7953.
31. Rakytska, T.; Truba, A.; Radchenko, E.; Golub, A. Manganese(II) Complexes with Schiff Bases Immobilized on Nanosilica as Catalysts of the Reaction of Ozone Decomposition. *Nanoscale Res. Lett.* **2015**, *10*, 472, https://doi.org/10.1186/s11671-015-1179-6.
32. Odularu, A.T. Manganese Schiff Base Complexes, Crystallographic Studies, Anticancer Activities, and Molecular Docking. *J. Chem.* **2022**, *2022*, 7062912, https://doi.org/10.1155/2022/7062912.
33. Nishi, T.; Nakada, M.; Hirata, M. Lattice parameter functions of $(Am_yU_{1-y})O_{2-x}$ based on XRD and XANES measurements. *J. Solid State Chem.* **2017**, *256*, 252-255, https://doi.org/10.1016/j.jssc.2017.09.011.
34. Nasiri, S.; Rabiei, M.; Palevicius, A.; Janusas, G.; Vilkauskas, A.; Nutalapati, V.; Monshi, A. Modified Scherrer equation to calculate crystal size by XRD with high accuracy, examples Fe_2O_3, TiO_2 and V_2O_5. *Nano Trends* **2023**, *3*, 100015, https://doi.org/10.1016/j.nwnano.2023.100015.
35. Abdel-fatah, S.M. Novel imine Complexes Incorporating Ca(II) and Mg(II) Cations: Synthesis and Antimicrobial Activity. *Sohag J. Sci.* **2025**, *10*, 524–528, https://doi.org/10.21608/sjsci.2025.427800.1317.
36. Nandaniya, B.K.; Das, S.P.; Chhuchhar, D.R.; Pithiya, M.G.; Khatariya, M.D.; Jani, D.; Dangar, K.B. Schiff base metal complexes: Advances in synthesis, characterization, and exploration of their biological potential. *Int. J. Chem. Stud* **2024**, *12*, 131-134.
37. Keypour, H.; Shayesteh, M.; Golbedaghi, R.; Chehregani, A.; Blackman, A.G. Synthesis, characterization, and X-ray crystal structures of metal complexes with new Schiff-base ligands and their antibacterial activities. *J. Coord. Chem.* **2012**, *65*, 1004-1016, https://doi.org/10.1080/00958972.2012.665904.
38. Diana, R.; Panunzi, B. The Role of Zinc(II) Ion in Fluorescence Tuning of Tridentate Pincers: A Review. *Molecules* **2020**, *25*, 4984, https://doi.org/10.3390/molecules25214984.
39. Obande, E.; Mamman, S.; Ojo, S.A.; Ukoha, P.O. Antimicrobial Properties of Cu(I) and Cu(II) Complexes of a Schiff Base Ligand. *Int. J. Res. Sci. Innov.* **2024**, *11*, 502–513, https://doi.org/10.51244/IJRSI.
40. Khan, M.W.; Mishra, R.P.; Patel, B.; Patel, S.; Gupta, S.; Sen, S. Synthesis, Characterization, Swiss ADME and Antimicrobial Activity of Copper (II) Complex with 2-Sulfanilamidopyrimidine: Through DFT Spectroscopic with Profound Biological Implications. *Asian J. Appl. Chem. Res.* **2021**, *9*, 16-32, https://doi.org/10.9734/ajacr/2021/v9i130203.
41. Waziri, I.; O. Wahab, O.; A. Mala, G.; O. Oselusi, S.; A. Egieyeh, S.; Nasir, H. Zinc(II) complex of (Z)-4-((4-nitrophenyl)amino)pent-3-en-2-one, a potential antimicrobial agent: synthesis, characterization, antimicrobial screening, DFT calculation and docking study. *Bull. Chem. Soc. Ethiop.* **2023**, *37*, 633-651, https://doi.org/10.4314/bcse.v37i3.8.

42. Gomes da Silva Dantas, F.; Araújo de Almeida-Apolonio, A.; Pires de Araújo, R.; Regiane Vizolli Favarin, L.; Fukuda de Castilho, P.; De Oliveira Galvão, F.; Inez Estivalet Svidzinski, T.; Antônio Casagrande, G.; Mari Pires de Oliveira, K. A Promising Copper(II) Complex as Antifungal and Antibiofilm Drug against Yeast Infection. *Molecules* **2018**, *23*, 1856, https://doi.org/10.3390/molecules23081856.
43. Wani, M.Y.; Ahmad, A.; Malik, M.A.; Sobral, A.J.F.N. Mononuclear transition metal complexes containing iodo-imidazole ring endowed with potential anti-*Candida* activity. *Med. Chem. Res.* **2016**, *25*, 2557-2566, https://doi.org/10.1007/s00044-016-1653-4.
44. Kabeer, H.; Hanif, S.; Arsalan, A.; Asmat, S.; Younus, H.; Shakir, M. Structural-Dependent N,O-Donor Imine-Appended Cu(II)/Zn(II) Complexes: Synthesis, Spectral, and in Vitro Pharmacological Assessment. *ACS Omega* **2020**, *5*, 1229-1245, https://doi.org/10.1021/acsomega.9b03762.
45. Pinheiro, A.C.; Nunes, I.J.; Ferreira, W.V.; Tomasini, P.P.; Trindade, C.; Martins, C.C.; Wilhelm, E.A.; Oliboni, R.D.; Netz, P.A.; Stieler, R.; Casagrande, O.D.; Saffi, J. Antioxidant and Anticancer Potential of the New Cu(II) Complexes Bearing Imine-Phenolate Ligands with Pendant Amine N-Donor Groups. *Pharmaceutics* **2023**, *15*, 376, https://doi.org/10.3390/pharmaceutics15020376.
46. Yang, Y.; Guo, L.; Tian, Z.; Gong, Y.; Zheng, H.; Zhang, S.; Xu, Z.; Ge, X.; Liu, Z. Novel and Versatile Imine-N-Heterocyclic Carbene Half-Sandwich Iridium(III) Complexes as Lysosome-Targeted Anticancer Agents. *Inorg. Chem.* **2018**, *57*, 11087-11098, https://doi.org/10.1021/acs.inorgchem.8b01656.
47. Gomes, R.N.; Silva, M.L.; Gomes, K.S.; Lago, J.H.G.; Cerchiaro, G. Synthesis, characterization, and cytotoxic effects of new copper complexes using Schiff-base derivatives from natural sources. *J. Inorg. Biochem.* **2024**, *250*, 112401, https://doi.org/10.1016/j.jinorgbio.2023.112401.
48. Laurent, R.; Maraval, V.; Bernardes-Génisson, V.; Caminade, A.-M. Dendritic Pyridine–Imine Copper Complexes as Metallo-Drugs. *Molecules* **2024**, *29*, 1800, https://doi.org/10.3390/molecules29081800.
49. Gul, N.S.; Khan, T.-M.; Chen, M.; Huang, K.-B.; Hou, C.; Choudhary, M.I.; Liang, H.; Chen, Z.-F. New copper complexes inducing bimodal death through apoptosis and autophagy in A549 cancer cells. *J. Inorg. Biochem.* **2020**, *213*, 111260, https://doi.org/10.1016/j.jinorgbio.2020.111260.
50. Pichilingue, P.A.; Shakir, A.R. Rituximab plus concurrent radiation therapy for the management of CD20 - positive peripheral T- cell lymphoma: A case report and review of literature. *Cancer Rep. Rev.* **2018**, *2*, 1–3, https://doi.org/10.15761/crr.1000160.
51. Babgi, B.A.; Domyati, D.; Abdellattif, M.H.; Hussien, M.A. Evaluation of the Anticancer and DNA-Binding Characteristics of Dichloro(diimine)zinc(II) Complexes. *Chemistry* **2021**, *3*, 1178-1188, https://doi.org/10.3390/chemistry3040086.
52. Mukherjee, D.; Reja, S.; Sarkar, K.; Fayaz, T.K.S.; Kumar, P.; Kejriwal, A.; Das, P.; Sanphui, P.; Kumar Das, R. In vitro cytotoxicity activity of copper complexes of imine and amine ligands: A combined experimental and computational study. *Inorg. Chem. Commun.* **2022**, *146*, 110190, https://doi.org/10.1016/j.inoche.2022.110190.

Publisher's Note & Disclaimer